ELSEVIER

Chemical Geology 158 (1999) 257–269

CHEMICAL GEOLOGY
INCLUDING
ISOTOPE GEOSCIENCE

Evidence of bacterial activity from micrometer-scale layer analyses of black-smoker sulfide structures (Pito Seamount Site, Easter microplate)

Chrystèle Verati [a,*,1], Philippe de Donato [b,2], Daniel Prieur [c,d,3], Joël Lancelot [a]

[a] *Laboratoire de Géochimie Isotopique, UMR 5567 CNRS, Université Montpellier II, ISTEEM, cc 066, place E. Bataillon, 34095 Montpellier, cedex 05, France*

[b] *Laboratoire Environnement et Minéralurgie (LEM), UMR 7569 CNRS, ENSG-INPL, rue du Doyen Roubault-BP 40-54501 Vandoeuvre-les-Nancy cedex, France*

[c] *CNRS, UPR 9042, BP 74, 29 682 Roscoff cedex, Brest, France*

[d] *Université de Bretagne Occidentale, Brest, France*

Received 10 September 1997; received in revised form 9 March 1999; accepted 9 March 1999

Abstract

We report the observation of an external layer, less than 20 μm thick, attached to hydrothermal chimney fragments of black smokers collected from the Pito Seamount site on the Easter microplate. Scanning electron microscope observations revealed bacterial imprints located on and within the layer, which was associated with underlying layers of thin jarosite deposits and iron sulfides displaying corrosion features. X-ray, electron microprobe, DRIFT and HPLC measurements were used to determine the precise chemical composition and nature of compounds in the layer. The external layer was composed mainly of a combination of hydrated ferric sulfate, ferrous sulfate, iron oxi-hydroxide and elemental sulfur species. A jarosite-like mineral was found deeper in the layer. We suggest that this layer may not be the result of an abiotic thermochemical precipitation, but instead, was formed chemically by bacterial processes. These processes were (1) elemental sulfur oxidation which represents major energetic exchanges within the external layer and (2) bioleaching processes inducing iron oxidation. Originally, elemental sulfur probably resulted from thermochemical precipitation. The results of this study give new insight on the possible role and impact of related acidophilic microorganisms living in hot vent environments of the deep sea.

Keywords: Hydrothermal; Biomineralization; Bioleaching; Thiobacillus; Acidianus; Sulfides

1. Introduction

Because of the insights they may yield on the origin of life (Corliss et al., 1981; Deming and Baross, 1993; Forterre et al., 1995; Russell and Hall, 1997), studies of deep-sea microorganisms living in

* Corresponding author. UMR Géosciences Azur CNRS, UNSA, Parc Valrose, 06108 Nice Cedex 2, France. Tel.: +33-4-04926589; fax: +33-4-92076816; e-mail: verati@unice.fr

[1] E-mail: lancelot@dstu.univ-montp2.fr.

[2] E-mail: dedonato@ensg.u-nancy.fr.

[3] E-mail: prieur@sb-roscoff.fr.

0009-2541/99/$ - see front matter
PII: S0009-2541(99)00054-6

hydrothermal environments have intensified during recent years (Prieur et al., 1995; Stetter, 1996). Under extreme conditions that can include high temperature, high pressure and acidic pH, some bacteria are involved in mineral dissolution (Tuttle, 1985; Eberhard et al., 1995) or mineral growth (Juniper and Fouquet, 1988) by catalysing, controlling and influencing the kinetics of these processes. Potential habitats for bacterial growth are the external surfaces and porous structures of the hydrothermal chimneys (Baross and Deming, 1985; Jannasch and Wirsen, 1985; Winn et al., 1986; Wirsen et al., 1993). In the immediate vicinity of vent fluids, attached bio-constructions derived from microbial activity are typically described as centimeter-thick mats which may also be metal encrusted (Jannasch and Wirsen, 1981; Baross and Deming, 1985; Jannasch et al., 1989; Juniper and Tebo, 1995). Our observations document additional types of micrometer-scale microbial structures that cover external surfaces of a sulfide chimney. This work focuses on the study of structural and chemical compositions of an external layer in order to understand its origin and to provide a model for its formation.

2. Location and samples analyzed

The site of Pito Seamount is centered on 23°19′S–111°38′W on the Easter microplate in the southeast Pacific (Fig. 1). It is located north of the East rift propagator, on the eastern boundary of the Easter microplate. During dives with the Nautile

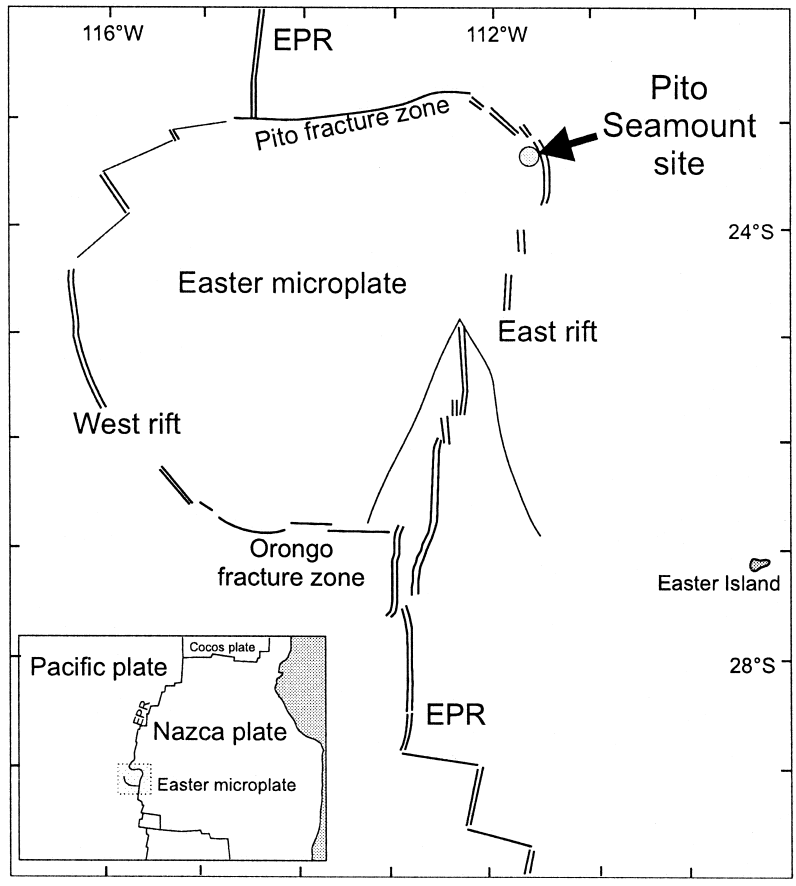

Fig. 1. Location of the hydrothermal site at Pito Seamount in the southeast Pacific (modified after Francheteau et al., 1988). Double lines: spreading center; single line: transform fault.

submersible, active black smokers were discovered in November 1993 at a depth of 2243 m (Francheteau et al., 1994) at the base of the seamount, which may be serving as a focal point for a new seafloor spreading axis to develop (Naar et al., 1997). Fluid temperatures are believed to be hot (> 200°C) although

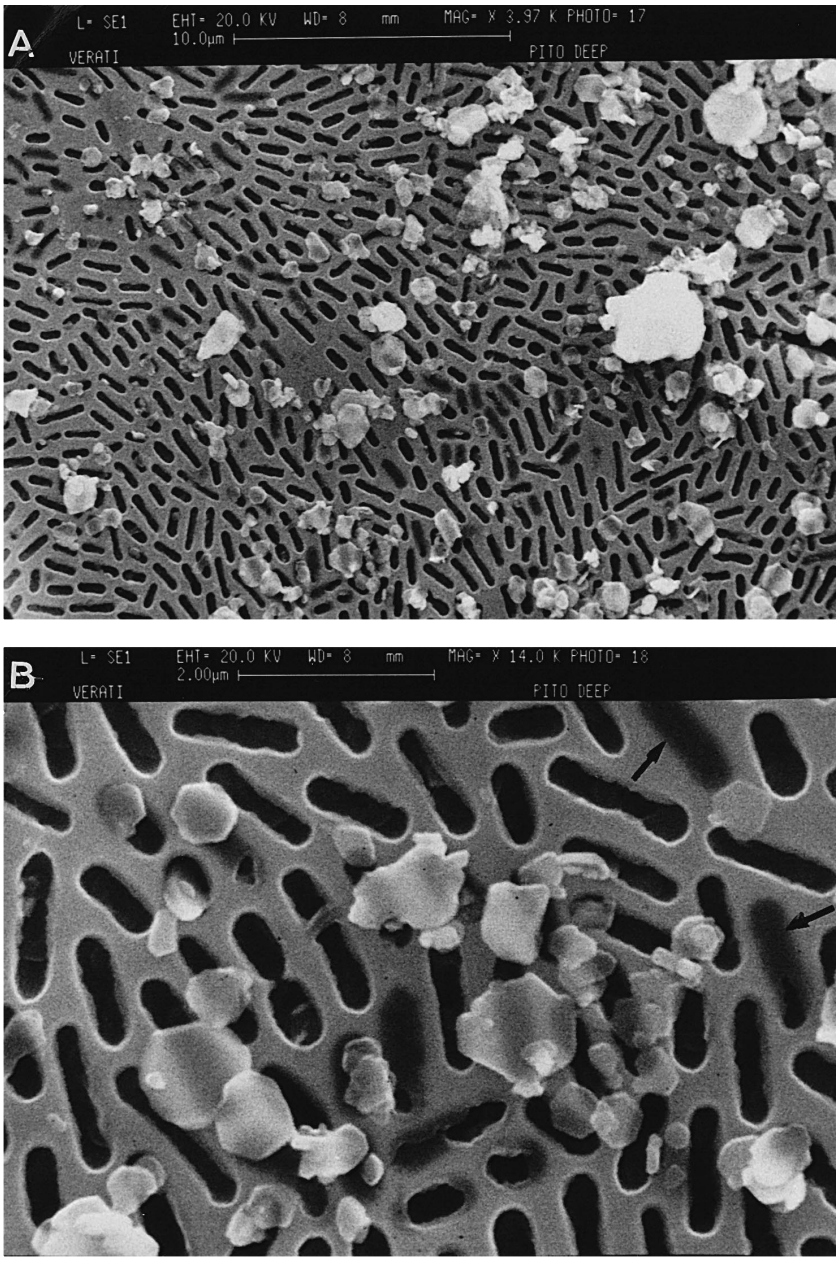

Fig. 2. (A) SEM photograph of the surface of the external layer: general view showing the high density of microbial imprints. Bar = 10 μm. (B) Detail from A, showing Fe-oxides with a hexagonal forms (hematite) and the apparent imprint of a dividing cell near the center of the photo. Note the presence of imprints remaining visible under very thin layer (arrows). Bar = 2 μm (imprints are about 0.6 μm in diameter and 1–2 μm in length).

there were no direct temperature measurements (Naar et al., 1997). The biological community was undiversified and composed of alvinellid worms, crabs, shrimps and actinides (Naar et al., 1997).

Studied samples are external fragments of a chimney (samples PI0710a and PI0710b) collected using a hydraulic grab sampler. Samples were not particularly handled in anticipation of microbiological studies, since dives were dedicated to geophysical experiments. For technical reasons, only a few fragments of external chimney were collected.

Subhedral pyrite and sphalerite constitute the major mineral phases, in association with amorphous silica and anhydrite. Based on the paragenesis, ambient fluid temperature was around 50–150°C at the time of mineral precipitation. Determining the actual temperature of these external fragments in situ is difficult due to the possible fluctuations of the temperature gradients within the chimney wall and surficial mixing with cold seawater. Using a binocular microscope, we observed a remarkable, very thin layer strictly located on the outer part of irregularly shaped chimney fragments. Macroscopically, the external layer varied in color from red to orange, with a shiny luster brittle texture, and without any crystalline structures. Thin yellow deposits were observed infrequently between this layer and the sulfides.

3. SEM observations and X-ray analyses

3.1. The external layer

Scanning electron microscope (SEM) observations revealed a layer 1–20 μm thick. This layer was densely dotted by numerous micro-perforations about 1 μm long of constant, elongated shape with rounded terminations (Fig. 2). A high concentration of empty cavities, nearly 150 million per cm^2, was visible on the surface of the layer, and some cavities were observed within the layer itself (Fig. 2). Furthermore, these high-resolution observations enabled us to identify individual hexagonal iron oxide crystals lying on the surface (hematite: Fe_2O_3). Polished samples of the same external layer displayed a transversal section where empty cavities were preserved across the thickness, with major sub-circular forms with some elongated ones (not shown).

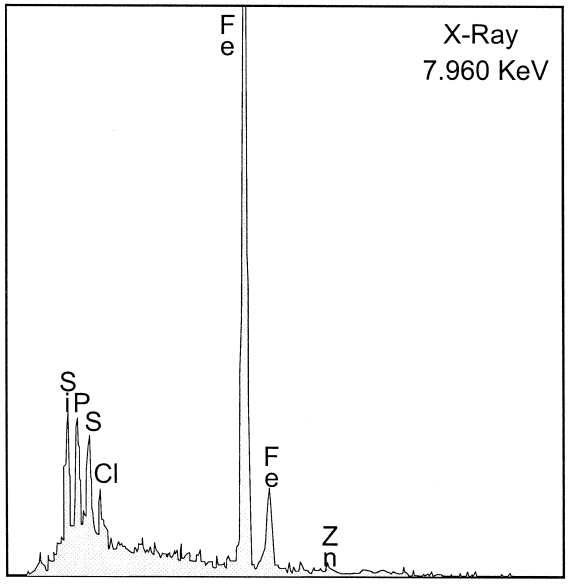

Fig. 3. Energy-dispersive X-ray spectrum of the external layer (without Fe-oxide interferences).

An energy-dispersive spectrometric (EDS) analyser connected to the SEM provided qualitative X-ray analyses of hematite-free portions of the layer, revealing that Fe was the major component and that S, Si, Cl, Zn and P were present in lesser proportions (Fig. 3).

3.2. Sulfide substrate

Observations of sulfides that are the substrate to the external iron-bearing layer showed a typical hydrothermal paragenesis, but some corrosive perforation of uniform diameter on colloform iron sulfides was observed (Fig. 4). In addition, rare yellow deposits between sulfides and the external Fe-bearing layer were composed of numerous micrometer crystals. Qualitative X-ray analyses identified these minerals as jarosite-like sulfates ($KFe_3(SO_4)_2(OH)_6$).

4. Electron microprobe analyses

Quantitative electron microprobe analyses on polished samples of the external layer provided the proportions of 13 elements, including oxygen. The results of 22 individual analyses are summarized in

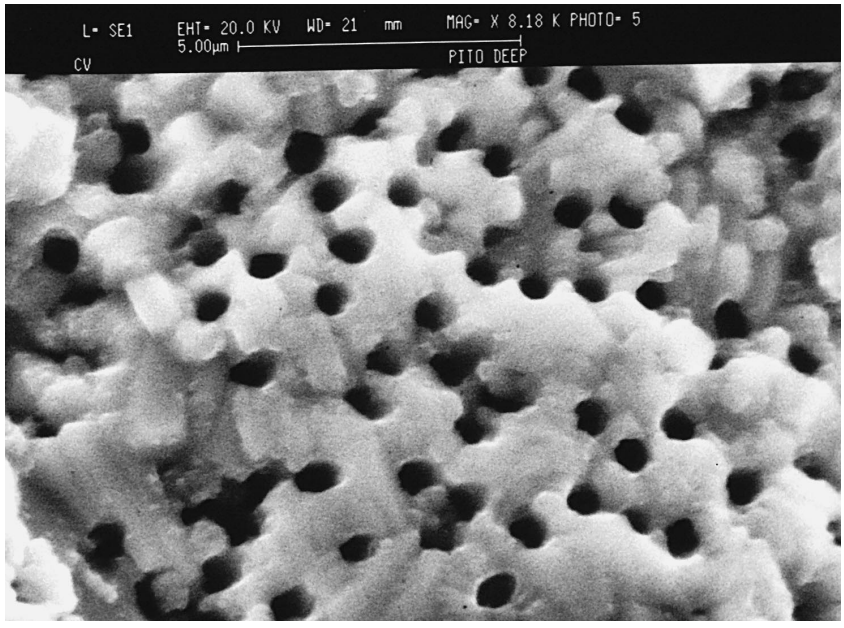

Fig. 4. SEM photograph of biocorrosion phenomenon occurring on the iron sulfide substrate. Note the regular size of each hollow. Bar = 5 µm.

Table 1. Analytical totals ranged from 73% to 80%, never approaching 100%, probably because of H_2O content in the layer. According to our previous qualitative SEM analyses, Fe is the predominant element; Si, P, S contents reach 4% each. Oxygen, with an average content of 20%, and iron are thus the major components. Other elements were also detected: three layer analyses revealed a significant As content and all analyses showed a constant Zn content close to 1%. The remaining elements (Na, Pb, K, Ca, Ni, Cu) were not detected or were close to the analytical detection limit.

Similar electron microprobe analyses were performed on the sulfates underlying the external layer (Table 2). The results confirm that K-sulfate crystals were jarosite-like minerals enriched in Zn and Si.

5. DRIFT and HPLC measurements

Diffuse reflectance infrared Fourier transform spectroscopy (DRIFTS) combined with a selective high pressure liquid chromatographic desorption method (UV-HPLC) is a powerful way to investigate the nature, amount and spatial distribution of iron and sulfur chemical species on mineral surfaces during experimental bioleaching processes (De Donato et al., 1993).

First of all, a gentle dry mechanical breaking up step was applied to the chimney fragments. Such experimental conditions allow to preserve the initial chemical surface structure of the sample. Resulting divided particles were analyzed by DRIFTS (Bruker IFS 55 with Harrick attachment) and HPLC (Hewlett Packard 1081B) combined with Ultra Violet (UV) detection (Hewlett Packard 1040A).

DRIFT measurements on powdered minerals allow the determination of the nature of pellicular phases that appear during oxidation of sulfides. UV-HPLC measurements are used to quantitatively extract and identify the sulfur layers present on mineral surfaces. These combined analyses were performed, according to previously described protocols (De Donato et al., 1993), on a portion of chimney fragments where sulfides were well covered by the external layer.

5.1. DRIFT measurements

Diffuse reflectance infrared Fourier transform measurements were conducted both on the initial

Table 1
Electron microprobe analyses of the external thin layer polished section

No.	Na, %	As, %	Si, %	P, %	Pb, %	K, %	Ca, %	Zn, %	Cu, %	Ni, %	S, %	Fe, %	O, %	Total, %
1	–	–	1.1	–	–	–	0.1	0.7	–	–	3.5	51.1	19.6	76.2
3	–	–	1.6	0.3	–	–	0.2	0.8	–	–	2.6	50.8	19.6	75.9
4	–	–	1.1	–	–	–	0.2	0.7	–	–	3.7	49.6	19.4	74.6
5	–	–	1.1	–	–	–	0.2	0.8	–	–	3.8	49.9	19.6	75.4
6	–	–	1.2	–	–	–	0.2	0.8	–	–	3.5	47.8	18.8	72.3
7	–	–	1.2	–	–	–	0.2	0.8	–	–	3.9	48.8	19.6	74.5
8	–	2.6	3.7	3.5	0.1	–	0.3	1.2	–	–	1.2	41.1	22.1	75.9
9	–	0.1	4.0	2.3	–	–	0.3	1.2	–	–	1.8	43.4	22.2	75.5
10	–	–	1.3	0.1	–	–	0.1	0.6	–	–	2.9	50.4	19.1	74.5
12	–	–	1.5	0.2	0.1	–	0.1	0.9	–	–	3.2	51.6	20.1	77.7
13	–	–	1.2	–	–	–	0.1	0.6	–	–	3.0	52.1	19.6	76.8
14	–	–	0.8	0.1	–	–	0.1	1.3	–	–	3.4	51.1	19.4	76.2
15	–	–	1.1	1.1	0.1	0.1	0.1	1.5	–	–	3.2	48.7	20.3	76.3
22	–	–	0.7	–	0.1	0.2	–	2.1	–	–	3.8	47.7	18.9	73.6
23	–	–	1.0	0.1	–	0.1	–	2.0	–	–	4.2	50.7	20.5	78.6
26	–	–	1.0	1.1	–	–	0.1	0.5	–	–	2.7	51.6	20.2	77.3
27	–	–	0.9	0.1	–	–	0.1	0.8	–	–	2.7	53.7	19.5	77.8
28	–	–	0.5	0.1	–	–	0.1	0.5	–	–	3.2	53.4	19.3	77.1
29	–	–	0.5	0.1	–	–	0.1	0.5	–	–	3.2	52.8	19.2	76.4
30	–	–	1.2	–	–	–	0.1	0.6	–	–	3.2	51.3	19.5	75.9
31	–	–	1.1	–	–	–	0.1	0.5	–	–	3.5	50.4	19.3	74.9
35	–	–	3.9	2.9	–	0.1	0.2	0.7	–	–	1.8	46.2	23.5	79.9
Averages														
	nd	0.1	1.4	0.5	< 0.1	< 0.1	0.1	0.9	nd	nd	3.2	50.0	20.0	

Analyses were performed on different hand-picked fragments. The bottom row in table represents the analytical average. (–: not detected (nd); analytical detection limit = 0.1%).

sample and after the chromatographic sequence. A diffuse reflectance spectrum (2000–600 cm^{-1}) of the initial sample is shown in Fig. 5. The infrared profile results from the contribution of different components. The major product identified is ferric sulfate (typical bands at 1160, 1106, 627 and 608 cm^{-1}) that is partially hydrated (scissoring mode of the structural water around 1650 cm^{-1}). Minor contributions of hydrated ferrous sulfate (shoulder at 987 cm^{-1} and band around 1616 cm^{-1}) and non-hy-

Table 2
Electron microprobe analyses of K-sulfate polished section

Na, %	As, %	Si, %	P, %	Pb, %	K, %	Ca, %	Zn, %	Cu, %	Ni, %	S, %	Fe, %	O, %	Total, %
–	–	0.4	0.1	–	3.6	0.1	1.3	–	–	8.1	38.7	20.9	73.3
–	–	0.1	0.1	–	5.8	–	1.1	–	–	10.4	31.3	21.0	69.9
–	–	0.1	0.1	–	5.8	–	1.2	–	–	10.4	30.6	20.8	68.9
–	–	0.7	–	–	0.1	0.1	1.6	–	–	3.6	52.2	19.9	78.2
–	0.1	0.1	0.1	–	5.6	–	1.3	–	–	10.6	30.5	21.1	69.4
–	–	0.1	–	–	5.5	–	1.3	–	–	10.3	31.5	20.9	69.8
Averages													
nd	< 0.1	0.2	< 0.1	nd	4.4	< 0.1	1.3	nd	nd	9.0	35.8	20.8	

Analyses were performed on an area ($\sim 100\ \mu m^2$) from a single fragment. The bottom row in table represents the analytical average. (–: not detected (nd); analytical detection limit = 0.1%).

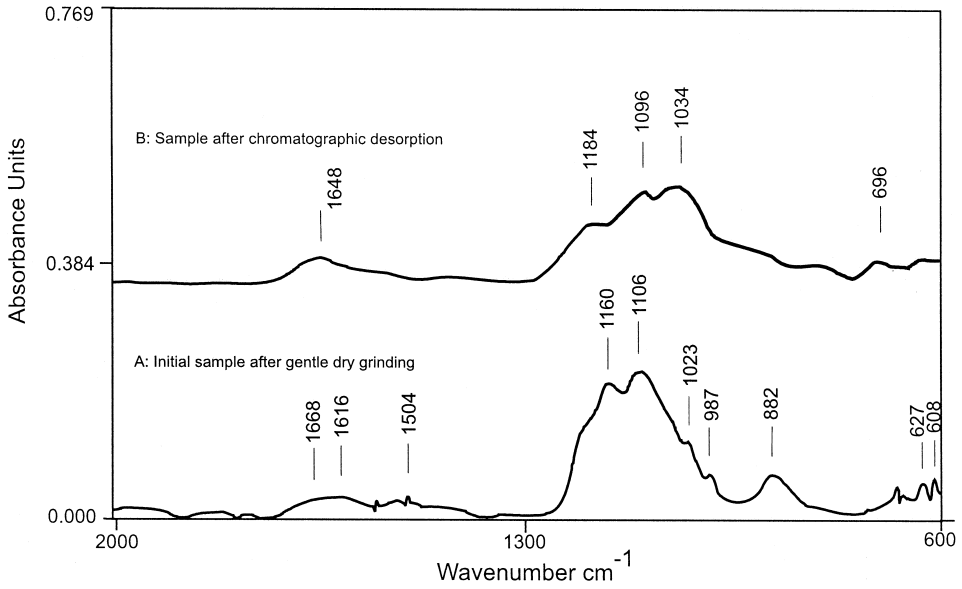

Fig. 5. DRIFT measurements: diffuse reflectance spectrum of the sample before (A) and after (B) the chromatographic sequence.

drated ferrous sulfate (shoulder at 987 cm^{-1}) was also observed. Moreover, a band at 882 cm^{-1} may be assigned to ferric oxi-hydroxide species. Taking into account the thickness of the layer (>10 μm) and the depth of penetration of the infrared radiation in the diffuse reflectance mode (less than the wavelength, <8 μm at 1200 cm^{-1}), all the infrared information are collected from the superficial layer of the sample. The composition of the substrate species cannot be reliably inferred under these conditions.

After the chromatographic sequence, the diffuse reflectance infrared profile of the sample was altered (Fig. 5). Changes in the infrared profile indicate that hydrated ferric and ferrous species were removed by elution with water and methanol solutions. This leads to a decrease of the thickness of the surface layer. Under these conditions, the infrared beam can reach more deeply into the bulk sample. The resulting infrared spectrum was very similar to typical jarosite type species (bands at 1648, 1184, 1096 and 1034 cm^{-1}). Displacement of the broad band (1300–1000 cm^{-1}), characteristic of the stretching vibration of S–O vibrators in sulfate structures, could indicate a residual contribution of ferrous sulfate. Because homogeneous dissolution of the layer cannot be controlled, it is difficult to know if the infrared information was derived entirely from the surface layer or if it also contained subsurface material. However, it can be assumed that the resulting infrared spectrum had a mixed surface layer–bulk origin.

5.2. HPLC and UV measurements

Even if the chromatographic device we used in this study has been described previously (De Donato et al., 1993), the main stages are recalled. The experimental set up consisted in a high pressure liquid chromatograph (HP1081B) connected with a diode array UV-visible spectrometer (HP1041A) operating between 190 and 600 nm (Fig. 6). The speed of the mobile phase was 0.3 ml min^{-1}. Detection parameter was optimized in order to take one UV spectrum (190–400 nm) every 10^{-2} s. Under these conditions, the chemical composition of each drops coming out of the chromatographic column can be analyzed. Quantitative determination of elemental sulfur was carried out using the established Beer–Lambert law for the two characteristic peaks (221 and 263 nm) for concentrations ranging between 10^{-6} and 10^{-3} mol l^{-1}.

The chromatographic column was filled with the sample after the fragmentation step. The mass of the solid phase was 0.77 g. Desorption procedure was

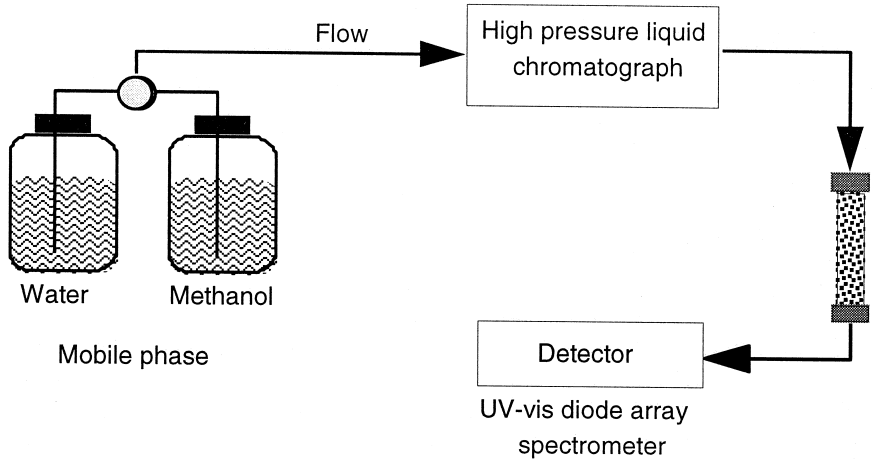

Fig. 6. Chromatographic device for HPLC and UV measurements.

conducted on the base of two different chromatographic sequences which link up one after the other. A first water desorption sequence was used to remove hydrophilic surface species such as polysulfides (S_nS^{2-}) and part of iron oxidized sulfates. Then, a methanol desorption sequence was used to remove hydrophobic surface species such as elemental sulfur. The chromatogram (at 263 nm) of methanol desorption is shown in Fig. 7. The increased absorbance at 263 nm, observed immediately after the dead volume of the column (0.2 min), is characteristic of the desorption of chemical species of the superficial layer of the sample. After 40 min, desorption was nearly complete. Full UV spectra taken after 4, 8, 19 and 40 min, respectively, are shown in Fig. 8. The same UV profiles were observed during

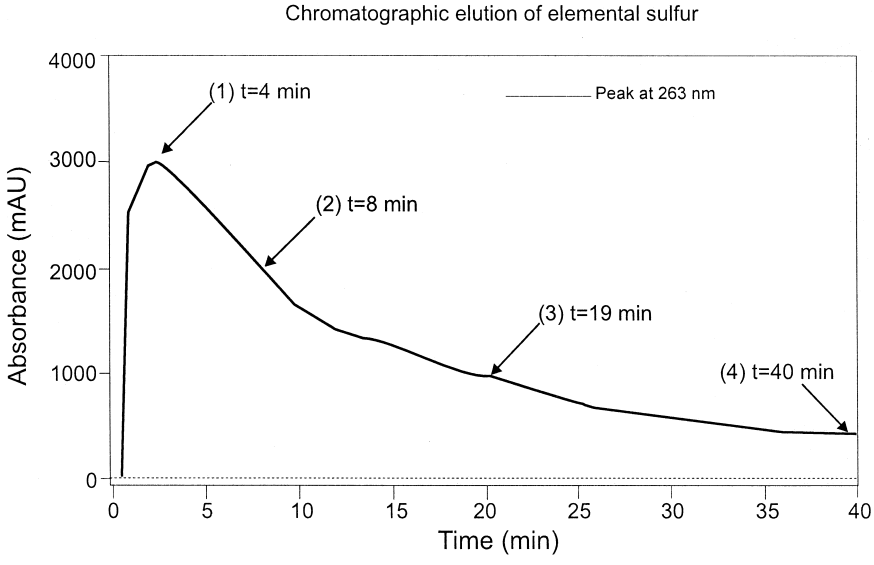

Fig. 7. HPLC measurements: chromatogram of methanol desorption at 263 nm versus time (mAU = milli Absorbance Unit).

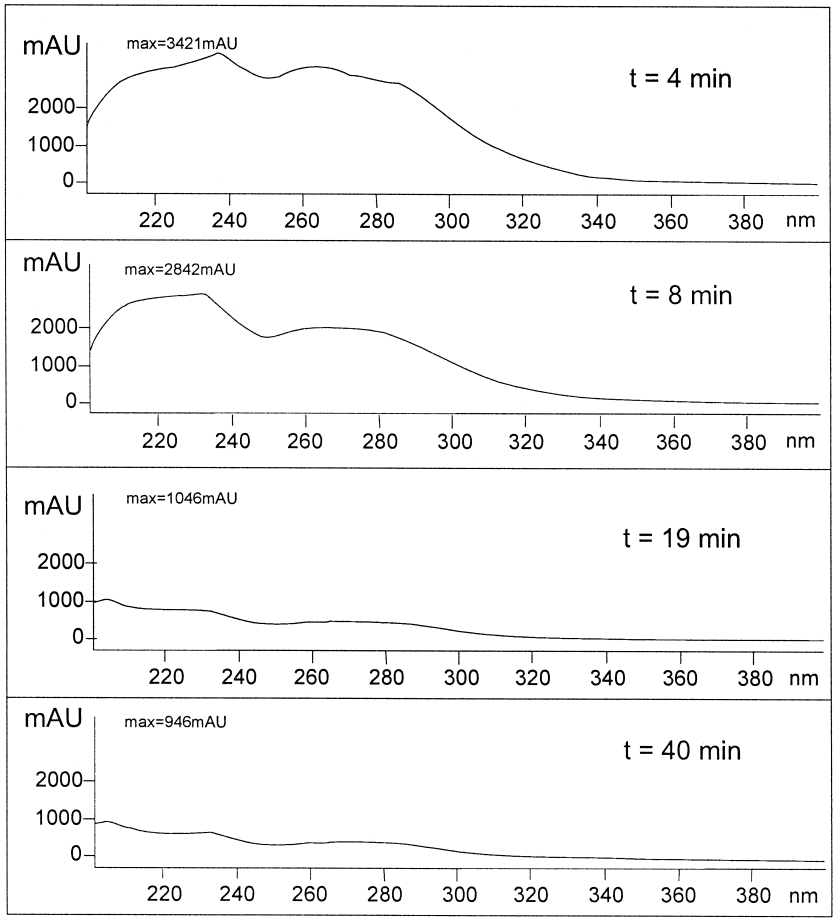

Fig. 8. HPLC measurements: full UV spectra taken at different periods (mAU = milli Absorbance Unit).

the entire desorption with absorption peaks at 221, 263 and 280 nm. The UV profiles related to the position of these peaks is characteristic of elemental sulfur in the S_8 form (ring of eight sulfur atoms) indicating that sulfur was the only compound removed from the surface of the sample. By integrating the chromatogram at 263 nm (Fig. 7) and using its specific molar extinction coefficient ($\varepsilon_{263} = 780$ mol^{-1} l cm^{-1}), the total desorbed amount of surface elemental sulfur was determined to be 79.8 μM g^{-1}. Taking into account the calculated mean cross-sectional area of sulfur (43 $Å^2$) (De Donato et al., 1993) and the measured specific surface area of the sample determinated by nitrogen adsorption (0.33 m^2 g^{-1}-BET method), the statistical surface coverage of elemental sulfur was equivalent to 61 layers. This result proves that elemental sulfur was an important component of the thick external layer on the SEM picture in Fig. 2.

6. Discussion

According to the analyses of this study, the external layer does not correspond to any known hydrothermal mineral phase. We provide the following evidence that it is produced directly or indirectly by bacterial oxidation. Firstly, the size and shape of the perforations in the layer fall within the range typical for rod-shaped bacteria. Such a hypothesis is strengthened by the observation of numerous perforations which appear to reflect bacterial division

once cell length approached 1.5 μm (Fig. 2). Similar imprints located within the layer also suggest that bacterial growth contributes to the progressive formation of the layer or that subsequent bacterial colonization keeps pace with growth of the sulfur layers that serve as an energy source. Secondly, the chemical composition of the external layer is a complex mixture. DRIFT measurements were in good agreement with SEM observations and confirmed that the mixed chemical nature of the layer involves major ferric sulfates, (mainly hydrated: $9H_2O$), minor ferrous sulfates (hydrated and non hydrated), iron oxi-hydroxides and elemental sulfur species. Similar iron enrichments have been described as a product of microbial activity on smoker walls (Baross and Deming, 1985). HPLC water desorption revealed that some of these species are hydrophilic and can be removed from the surface. The HPLC analyses of this study also showed that the external layer includes a major amount of elemental sulfur that is not chemically bound to the iron. However, the homogeneity of the layer shown in Fig. 2 indicates that the elemental sulfur and iron species are thoroughly intermixed.

At a bacteria–mineral interface, microbial metabolism could derive energy from thermodynamically favorable chemical reactions. One of the key parameters controlling bacterial activity and its location is the nature of the energetic substrates present on the chimney surfaces. The following discussion takes into account the most likely physico-chemical reactions which may take place at a microorganism–mineral interface, based on the chemical composition of the external layer. Because the corrosion patterns are limited mainly to the micrometer-scale layer, we first hypothesize that major energetic exchange took place in this layer, where elemental sulfur, the initial source of energy, was originally deposited by thermochemical processes. A description of this hypothetical biochemical interface is shown in Fig. 9.

6.1. Bioleaching process

The diameter of the bacteria-like imprints on the external layer compare well with the size of the perforations in colloform iron sulfides, suggesting that the holes in iron sulfides are also created through a bioleaching process by micro-organisms of very similar size. Moreover, the density of corrosion patterns are similar to those obtained on pyrite after 30–40 days of bioleaching (De Donato et al., 1991) and the absence of overlapping holes suggests either a recently bioleached mineral or a limited bio-oxidation process. Because the corrosion patterns are limited mainly to the micrometer-scale external layer, the bioleaching at the sulfide surface appears to be a secondary-reaction energetic interface. The bacterial oxidation of sulfides may occur through (1) a direct mechanism where bacteria adhere to the mineral surface and dissolves the mineral or (2) an indirect mechanism of solubilization where adhesion is not required. Such corrosion patterns characterize a propagating pore mechanism in which the reactive interface is the bottom of the pores and the remaining surfaces within the bioleached tunnel are not always chemically active (Mustin et al., 1992). Products of bioleaching are primarily ferric sulfate species which accumulate progressively in the external layer (see reactions 2 and 3 in Fig. 9).

6.2. Sulfur bio-oxidation in the external layer

Secondary bacterial or chemical mechanisms by themselves cannot explain the large amount of elemental sulfur detected in the external layer. We hypothesize that bacterial colonization in the external layer keeps pace with a thin surface of elemental sulfur that is continually deposited on substrate sulfide surfaces. This elemental sulfur surface could serve as a rich source of energy for the microorganisms. For example, an elemental sulfur surface provides a more energetic substrate for Thiobacilla ($\Delta G^\circ = -188$ kcal mole^{-1} for S_o/S^{+VI}) than does iron oxidation (Fe^{+II}/Fe^{+III}) ($\Delta G^\circ = -8.37$ kcal mole^{-1}) during bioleaching processes (Lundgren and Tano, 1978). Elemental sulfur bio-oxidation (see reaction 1, Fig. 9) could account for 90% of energetic exchange taking place at the mineral–bacteria interface, whereas iron oxidation (see reaction 2, Fig. 9) only 10%. Sulfur bio-oxidation produced SO_4^{2-} ions (reaction 1 in Fig. 9). Secondary mechanisms of some elemental sulfur formation in the external layer could have involved chemical (oxidation of the mineral by dissolved O^2, Fe^{3+}, see reaction 4 and 5 in Fig. 9) and electrochemical reactions (partial anodic

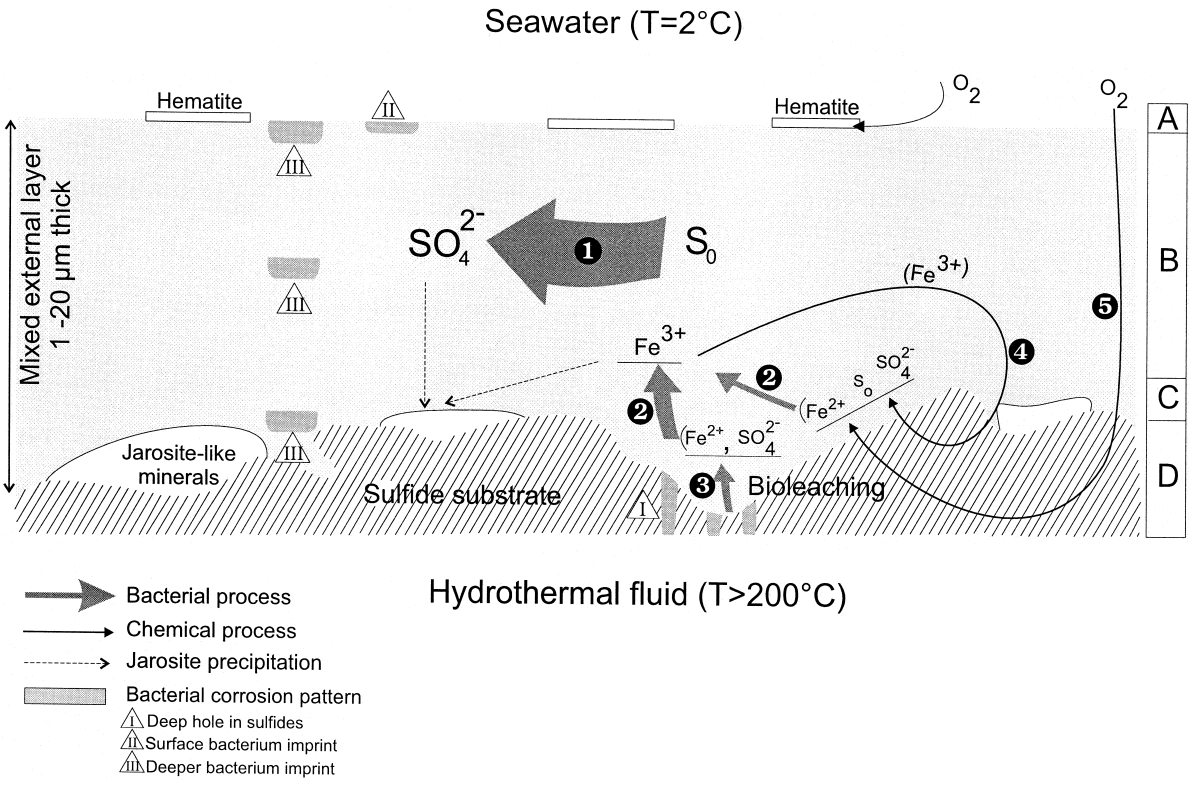

Fig. 9. Schematic of the bio-chemical interface in black-smoker environments. A, C and D indicate major mineral species in each depth interval: A = hematite crystals on the external layer, B = external layer, C = jarosite-like deposits and/or jarosite-like mineral found deeper in the layer, D = sulfide substrate. Reaction 1 is the major bacterial process occurring at this micro-organism/mineral interface. Reactions 2 and 3 are related to typical oxidation of pyrite by bacteria, including jarosite precipitation. Reactions 4 and 5 are related to abiotic chemical processes.

Oxidation of sulfur by bacteria

1: $S_o + 3/2O_2 + H_2O \rightarrow SO_4^{2-} + 2H^+$

Oxidation of pyrite by bacteria (Ehrlich, 1996)

2: $2Fe^{2+} + 0.5O_2 + 2H^+ \rightarrow 2Fe^{3+} + H_2O$

3: $FeS_2 + 3.5O_2 + H_2O \rightarrow Fe^{2+} + 2H^+ + 2SO_4^{2-}$

Oxidation of the mineral by dissolved O_2 and Fe^{3+}.

4: $14Fe^{3+} + FeS_2 + 8H_2O \rightarrow 15Fe^{2+} + 2SO_4^{2-} + 16H^+$ with $SO_4^{2-} \rightarrow (S_o)$.

5: $FeS_2 + 2H^+ + 0.5O_2 \rightarrow Fe^{2+} + 2(S_o) + H_2O$

reaction of the mineral). Moreover, strains of Thiobacilla are known to (1) produce sulfur detectable outside the cell when they grow on thiosulfate or sulfide and (2) accumulate fine sulfur deposits inside the cell wall (Hazeu et al., 1988).

6.3. Microorganisms inhabiting the micro-layer

The combined processes of pyrite corrosion and ferrous iron and sulfur oxidation can be attributed to the activities of sulfur-oxidizing bacteria. For instance, the mesophilic (30–35°C) and acidophilic (pH = 2–4) *Thiobacillus ferrooxidans* is an obligate autotroph able to derive energy from the oxidation of ferrous iron, as well as of sulfur and reduced sulfur compounds (Kuenen et al., 1992). *T. thiooxidans* derives energy from the oxidation of elemental sulfur (Garcia et al., 1995). *Acidianus brierleyi* is a thermophilic (75°C) and acidophilic (pH = 1–2) archaebacterium with the ability to grow by leaching sulfides following adsorption onto the mineral surface (Brierley and Brierley, 1973; Blöchl et al., 1995, Konishi et al., 1995). Striking similarities exist

between the external layer of this study and a coarse pellicular phase appearing on pyrite during oxidation by *T. ferrooxidans*, as well as between the corrosion figures on the colloform iron sulfides of this study and cracks 0.6 μm-wide observed on the surface of pyrite (De Donato et al., 1991; Monroy Fernandez et al., 1995). However, experimental studies of *T. ferrooxidans* have never produced such well developed structures as those observed here (Fig. 2). Thus, essential in situ parameters may control bacterial activity in black-smoker environments; e.g., the preexistence of a thin superficial sulfur layer, the duration of the bioleaching process or fluctuation in hydrothermal fluxes.

6.4. Model and summary

The most probable biogeochemical interactions occurring between hydrothermal mineral paragenes-es, jarosite-like species, and the external layer are summarized in Fig. 9.

Bacterial imprints within a newly discovered mineral layer on smoker walls provide evidence for prior existence of a large number ($\sim 10^8$ cm^{-2}) of microorganisms in the layer. We hypothesize that microorganisms resembling *T. ferrooxidans*, *T. thiooxidans*, *A. brierleyi* or other oxidizing bacteria are responsible for the bioleaching process on the iron sulfides, as well as for sulfur oxidation in the external layer. The absence of rod-shaped bacterial cells from the sampled micrometer-scale layers may be explained by (1) no application of chemical fixatives during sample collection and storage, (2) in situ fluctuations during successive pulses of hydrothermal fluids as well as migration of the thermal gradient within the black-smoker walls, or (3) absence of bacterial adhesion.

During the first step of the sulfide bioleaching process, microorganisms adhering to the sulfide surface initiate the solubilization of ferrous iron and sulfate. In the second step, unattached microorganisms oxidize Fe^{2+} to Fe^{3+} in the leachate. Simultaneously, adsorbed bacteria oxidize elemental sulfur in the primary superficial layer and induce the observed imprints. For simplicity, only these three different steps are shown in Fig. 9. Production of the external layer corresponds to a progressive accumulation of all the bio-oxidation products; although, local elemental sulfur accumulation may be the result of indirect chemical oxidation through ferric ions and dissolved oxygen. Hematite crystals on the external layer may represent an oxidation product of seawater interaction. The presence of jarosite deposits located deeper in the layer and/or directly on the surface of the sulfide substrate can be explained by (1) an early precipitation of a portion of the ferric iron with SO_4^{2-} as a result of microbial sulfide dissolution and oxidation (reactions 2 and 3, Fig. 9), and (2) a precipitation of ferric iron and SO_4^{2-} in excess produced mainly by elemental sulfur oxidation (reaction 1, Fig. 9) during the entire process.

Microorganisms attached to the mineral surfaces may grow in a micro-environment that constitutes an interface adequate for profitable bio-oxidation. Further investigations on additional hydrothermal mineral samples may help to confirm or refine our hypothesis and would clarify whether such micrometer layers are widespread at active hydrothermal sites or if this phenomenon is restricted to very local and perhaps ephemeral conditions.

Acknowledgements

We are thankful to the Captain, officers, and crew of the R.V. Nadir as well as to the Nautile team for their help during the 'Pito Cruise'. The Pito Cruise was jointly sponsored by IFREMER and INSU, and organized by UBO (Université de Bretagne Occidentale). We are thankful to D.F. Naar, J. Francheteau (Chief Scientists) and R. Hékinian for providing the samples, and to B. Nelson and the two anonymous reviewers for improving the English. *[MB]*

References

Baross, J.A., Deming, J.W., 1985. The role of bacteria in the ecology of black-smoker environments. Biological Soc. Washington Bull. 6, 355–371.

Blöchl, E., Burggraf, S., Fiala, G., Lauerer, G., Huber, G., Huber, R., Rachel, R., Segerer, A., Stetter, K.O., Völkl, P., 1995. Isolation, taxonomy and phylogeny of hyperthermophilic microorganims. World J. Microbiol. Biotechnol. 11, 9–16.

Brierley, C.L., Brierley, J.A., 1973. A chemolithoautotrophic and thermophilic microorganism isolated from an acidic hot spring. Can. J. Microbiol. 19, 193–198.

Corliss, J.B., Baross, J.A., Hoffman, S.E., 1981. An hypothesis

concerning the relationship between submarine hot springs and the origin of life on Earth. Oceanologica Acta no. SP: 59–69.

De Donato, P., Mustin, C., Berthelin, J., Marion, P., 1991. An infrared investigation of pellicular phases observed on the pyrite by Scanning Electron Microscopy, during its bacterial oxidation. C.R. Acad. Sci. Paris, t. 312, serie II: 241–248.

De Donato, P., Mustin, C., Benoit, R., Erre, R., 1993. Spatial distribution of iron and sulphur species on the surface of pyrite. Appl. Surf. Sci. 68, 81–93.

Deming, J.W., Baross, J.A., 1993. Deep-sea smokers: windows to a subsurface biosphere?. Geochim. Cosmochim. Acta 57, 3219–3230.

Eberhard, C., Wirsen, C.O., Jannasch, H.W., 1995. Oxidation of polymetal sulfides by chemolithoautotrophic bacteria from deep-sea hydrothermal vents. Geomicrobiol. J. 13, 145–164.

Ehrlich, H.L., 1996. How microbes influence mineral growth and dissolution. Chem. Geol. 132, 5–9.

Francheteau, J., Patriat, P., Segoufin, J., Armijo, R., Doucoure, M., Yelles-Chaouche, A., Zukin, J., Calmant, S., Naar, D.F., Searle, R.C., 1988. Pito and Orongo fracture zones: the northern and southern boundaries of the Easter microplate (southeast Pacific). Earth Planet. Sci. Lett. 89, 363–374.

Francheteau, J., Naar, D.F., Scientific Party, 1994. Black-smokers discovered, Pito Seamount, near Easter microplate propagator tip. EOS, Spring Meeting, 322.

Forterre, P., Confalonieri, F., Charbonnier, F., Duguet, M., 1995. Speculations on the origin of life and thermophily: review of available information on reverse gyrase suggest that hyperthermophilic procaryotes are not so primitive. Origin of life and evolution of the Biosphere 25, 235.

Garcia, O., Jerry, J.R., Bigham, J.M., Tuovinen, O.H., 1995. Sphalerite oxidation by *Thiobacillus ferrooxidans* and *Thiobacillus thiooxidans*. Can. J. Microbiol. 41, 578–584.

Hazeu, W., Batenburg-Van der Vegte, W.H., Bos, P., Van der Pas, R.K., Kuenen, J.G., 1988. The production and utilization of intermediary elemental sulfur during the oxidation of reduced sulfur compounds by *Thiobacillus ferrooxidans*. Arch. Microbiol. 150, 574–579.

Jannasch, H.W., Wirsen, C.O., 1981. Morphological survey of microbial mats near deep-sea thermal vents. Appl. Environ. Microbiol. 41, 528–538.

Jannasch, H.W., Wirsen, C.O., 1985. The biochemical versatility of chemosynthetic bacteria at deep-sea hydrothermal vents. Biological Soc. Washington Bull. 6, 325–334.

Jannasch, H.W., Nelson, D.C., Wirsen, C.O., 1989. Massive natural occurrence of unusually large bacteria (Beggiatoa sp.) at hydrothermal deep-sea vent site. Nature 342, 834–836.

Juniper, S.K., Fouquet, Y., 1988. Filamentous iron-silica deposits from modern and ancient hydrothermal sites. Can. Mineralogist 26, 859–869.

Juniper, S.K., Tebo, B., 1995. Microbe–metal interactions and mineral deposition at hydrothermal vents. In: Karl, D.M. (Ed.), The Microbiology of Deep-Sea Hydrothermal Vents. CRC Press, Boca Raton, 219–253.

Konishi, Y., Yoshida, S., Asai, S., 1995. Bioleaching of pyrite by acidophilic thermophile *Acidianus brierleyi*. Biotechnol. Bioeng. 48, 592–600.

Kuenen, J.G., Robertson, L.A., Tuovinen, O.H., 1992. The genera Thiobacillus, Thiomicrospira, and Thiosphaera. In: Balows, A., Trüper, H.G., Dworkin, M., Harder, W., Schliefer, K.H. (Eds.), The Prokaryotes, 2nd edn. Springer-Verlag, pp. 2638–2650.

Lundgren, D., Tano, T., 1978. Structure-Fonction Relationships of Thiobacillus relative to ferrous iron and sulphide oxidation. In: Murr, E.L., Torma, A.E., Brierley, J.A. (Eds.), Metallurgical Applications and Bacterial Leaching and Related Microbiological Phenomena. Acad. Press, 152–156.

Monroy Fernandez, M.G., Mustin, C., De Donato, P., Barres, O., Marion, P., Berthelin, J., 1995. Occurrences at mineral–bacteria interface during oxidation of arsenopyrite by *Thiobacillus ferrooxidans*. Biotechnol. Bioeng. 46, 13–21.

Mustin, C., De Donato, P., Berthelin, J., 1992. Quantification of intragranular porosity formed in bioleaching of pyrite by *Thiobacillus ferrooxidans*. Biotechnol. Bioeng. 39, 1121–1127.

Naar, D.F., Hekinian, R., Segonzac, M., Francheteau, J., Pito Dive Team, 1997. Hydrothermal Venting at Pito Seamount near Easter Island. Submitted to Marine Geology, December.

Prieur, D., Erauso, G., Jeanthon, C., 1995. Hyperthermophilic life at deep-sea hydrothermal vents. Planet. Space Sci. 43, 115–122.

Russell, M.J., Hall, A.J., 1997. The emergence of life from iron monosulphide bubbles at a submarine hydrothermal redox and pH front. J. Geological Soc. London 154, 377–402.

Stetter, K.O., 1996. Hyperthermophilic procaryotes. FEMS Microbiol. Rev. 18, 149–158.

Tuttle, J.H., 1985. The role of sulfur-oxidizing bacteria at deep-sea hydrothermal vents. Biological Soc. Washington Bull. 6, 335–343.

Winn, C.D., Karl, D.M., Massoth, G.J., 1986. Microorganims in deep-sea hydrothermal plumes. Nature 320, 744–746.

Wirsen, C.O., Jannasch, H.W., Molyneaux, S.J., 1993. Chemosynthetic microbial activity at MidAtlantic Ridge hydrothermal vents sites. J. Geophysical Res. 98, 9693–9703.